Synthesis and characterization of Fe-Al-Ni ternary composite metal oxides as highly efficient adsorbent for fluoride removal from water

Bai Sun[a,b,*], Jie Zhang[a], Chenfeng Ding[a], Fangwen Xu[a], Yunming Cheng[a], Zhuo Tang[a], Fakang Pan[a,*], Jinyun Liu[c], Shuguang Zhu[a]

[a]Key Laboratory of Water Pollution Control and Wastewater Resource of Anhui Province, College of Environment and Energy Engineering, Anhui Jianzhu University, Hefei 230601, China, Tel. +86-551-63828252; Fax: +86-551-63828252; emails: bsun@mail.ustc.edu.cn (B. Sun), 67681054@qq.com (F. Pan), 1045441563@qq.com (J. Zhang), 838842021@qq.com (C. Ding), 2392276291@qq.com (F. Xu), 502283466@qq.com (Y. Cheng), 1341451826@qq.com (Z. Tang), zhushuguang@ahjzu.edu.cn (S. Zhu)
[b]Nano-Materials and Environmental Detection Laboratory, Hefei Institute of Physical Science, Chinese Academy of Sciences, Hefei 230031, China
[c]Key Laboratory of Functional Molecular Solids, Ministry of Education, College of Chemistry and Materials Science, Anhui Normal University, Wuhu 241002, China, email: jyliu@ahnu.edu.cn

ABSTRACT

The Fe-Al-Ni composite oxide was synthesized through a simple coprecipitation method. The adsorbent was characterized by using scanning electron microscopy, X-ray diffraction, Fourier transform infrared spectroscopy, zeta potential, and energy dispersive analysis of X-rays, and its defluoridation properties were investigated. Adsorption kinetics fitted well the pseudo-second-order model. The fluoride adsorption isotherm was well described by the Freundlich model. Moreover, when the initial fluoride concentration was 200 mg/L, the maximum adsorption capacity was calculated as 59.5 mg/g from the Langmuir model. It was found that the maximum removal rate was 93.6% at pH = 7, with an initial fluoride concentration of 10 mg/L. The co-existing anions indicate that chloride, sulfate, and nitrate don't have much effect on F⁻ adsorption, but phosphate and carbonate show a significant effect on F⁻ removal. It shows that the efficacy of the adsorbents still maintains high as being reused, indicating that the spent adsorbent is suitable for regeneration.

Keywords: Adsorption; Fluoride; Fe-Al-Ni composite oxide

1. Introduction

Groundwater is one of the most important water sources for basic requirements. Fluoride naturally occurs in groundwater from different natural sources, usually weathering/leaching of fluoride-rich rocks of aquifer [1]. Fluoride-contaminated groundwater is a worldwide problem because fluoride is considered to be a very harmful pollutant in drinking water. The excessive ingestion of fluoride causes dental/skeletal fluorosis, neurological damage, and thyroid disorders. The World Health Organization

(WHO) reported that approximately 748 million people globally were forced to consume contaminated drinking water, which could cause high mortality rates [2]. Over the years, the presence of fluoride in drinking water above permissible limits has attracted public health interest. Efforts are therefore being made to reduce fluoride concentration within the permissible limit of 1.5 mg/L in accordance with the WHO [3]. China has been suffering from endemic fluorosis in drinking water, there are still about 70 million people using excessive fluoride water, especially in northeast, north, and northwest China [4]. The production

* Corresponding author.

of industry, such as metal smelting, fluorine ore mining, chemical fertilizers, and pesticides, would produce high fluoride wastewater. Therefore, it is necessary to study the economical and efficient method of removing fluoride.

Nowadays, there were many methods to remove fluoride ions from drinking water, including nanofiltration [5], sedimentation [6], electrocoagulation [7,8], electrodialysis [9], reverse osmosis [10], adsorption [11], and ion exchange [12]. Compared to the others, adsorption is the most effective due to its environmentally friendly, inexpensive, easy to operate, simple to design, and highly efficient when the selected adsorbent material is suitable for fluoride removal [13]. The most widely used adsorbents for defluoridation are compounds or materials inhering aluminum, calcium, and magnesium. Aluminum is neurotoxic in nature, and residual aluminum in drinking water has been reported by researchers [14]. Zhao et al. [15] prepared a new type of magnetic nano adsorbent, which used hydrated alumina containing Fe_3O_4 nanoparticles ($Fe_3O_4@Al(OH)_3$ NPs) as the adsorbent. The adsorption capacity calculated by the Langmuir equation was 88.5 mg/g at pH = 6.5. Chai et al. [16] developed a new type of adsorbent by using sulfur-doped Fe_3O_4/Al_2O_3 nanoparticles as adsorbent. Langmuir model was used to calculate that the fluoride adsorption capacity was 70.4 mg/g at pH = 7.0. Mukhopadhyay et al. [17] reported the synthesis of Ce(IV)-incorporated hydrous Fe(III) oxide (CIHFO) and its application for fluoride adsorption from water at neutral pH.

In the presented study, a granular Fe-Al-Ni adsorbent (FAN) was prepared by a simple coprecipitation method. This adsorbent was characterized by scanning electron microscopy (SEM), X-ray diffraction (XRD), Fourier transform infrared spectroscopy (FT-IR), zeta potential, and energy dispersive analysis of X-rays (EDS). Adsorption kinetics and adsorption isotherm of adsorbent were investigated. Moreover, the effect on pH and co-existing anions were optimized to provide a suitable condition for F^- removal through batch tests. In comparison with conventional F^- adsorbents, the prepared FAN exhibited a high adsorption capacity at pH = 7, showing potential applications.

2. Experimental

2.1. Reagents and instruments

The reagents used in the experiment mainly include magnesium sulfate heptahydrate, sodium carbonate, sodium fluoride, acetic acid, sodium chloride, trisodium citrate, and sodium hydroxide; Anhydrous ethanol, analytical purity, Xilong Scientific Co., Ltd., (China). Deionized water was prepared by FST-TOP-A24 super pure water mechanism, Shanghai FuShiTe Instrument Equipment Co., Ltd., (China).

The instruments used in the experiment mainly include TG16K-II Table high-speed centrifuge, Shanghai ZhaoDi biotechnology Co.,Ltd., (China). RCT basic magnetic stirrer, EKA Instrument Equipment Co., Ltd., (China). DHG-9023A air drying box, Shanghai YiHeng Scientific Instrument Co., Ltd., (China). PHS-3C conductivity meter, Shanghai Instrument Co., Ltd., (China). CSB-F-2 fluoride ion-selective electrode, Chengdu RuiXin instrument Co., Ltd., (China). 9XL-1008 muffle furnace, Shanghai JingHong

Experimental Equipment Co., Ltd., (China). PHB-3 digital pH meter, Shanghai SanXin Instrument Factory, (China). The XRD patterns of the adsorbents were performed on a D/MaxIIIA X-ray diffractometer (Rigaku Co., Japan), by using Cu Kα ($\lambda K_{\alpha1}$ = 1.5418 Å) as the radiation source in the range of 5°–80°. SEM image of the adsorbent was obtained with an FEI Quanta 200 FEG field emission scanning electron microscopy. The EDS spectrum and elemental mapping were performed on a Zeiss Auriga microscope (Germany) equipped with an Oxford Inca X-Max 50 detector. The FT-IR spectra of the adsorbents before and after adsorption were recorded with a NEXUS-870 FT-IR spectrometer (Thermo Fisher Scientific in USA) in the range of 4,000–400 cm^{-1}. The zeta potentials of the adsorbent before and after adsorption were analyzed on a zetasizer nano zeta potential analyzer (Malvern Instruments Ltd., Britain).

2.2. Preparation of adsorbent

In this paper, the Fe/Al/Ni composite oxide were prepared by coprecipitation method with the characteristics of simple operation, short reaction time, and excellent product performance. $FeCl_3·6H_2O$, $AlCl_3·6H_2O$, and $NiCl_2·6H_2O$ were uniformly mixed with the molar ratio of n(Fe):n(Al):n(Ni) as 1:1:1, and 1 mol/L sodium hydroxide solution was added drop by drop to adjust the pH of the solution to 7 and produced precipitation. The final FAN composite was then washed several times alternately with deionized water and anhydrous ethanol, and finally freeze-dried and ground for sieving.

2.3. Batch adsorption experiments

In this study, the fluoride ion-selective electrode method commonly used in the laboratory was used for determination. According to the Nernst equation, the obtained experimental data were used to draw the standard curve of lnC_F^- (mg/L)~E (mV). To obtain a concentration of 1,000 mg/L fluorides standard solution. Dissolved 2.21 g of NaF in a beaker with 100 mL of ultra-pure water, and transferred it into a 1 L volumetric flask. All the solutions for fluoride removal experiments and analysis were prepared by diluting the stock solution to a given concentration with ultra-pure water. The calibration curve was calculated by the potential of the standard sodium fluoride solutions (1–50 mg/L) at pH = 7. The pH value was adjusted by using 0.1 mol/L HCl and NaOH solution.

The adsorption capacity, removal rate, and distribution coefficient (K_d) of fluoride ions were calculated by Eqs. (1)–(3), respectively.

$$q_e = \frac{(C_0 - C_e)V}{m} \tag{1}$$

$$\eta = \frac{(C_0 - C_e)}{C_0} \times 100\% \tag{2}$$

$$K_d = \left(\frac{C_0 - C_e}{C_e}\right)\frac{V}{W} \tag{3}$$

where C_0 and C_e represent the initial and equilibrium fluoride concentration (mg/L) respectively, V (mL) is the volume of solution, m (g) is the amount of the adsorbent, and W (g) is the mass of the adsorbent.

In the isothermal adsorption experiment of the adsorbent on fluoride, the adsorbent was added to the 50 mL plastic centrifugal tube, and a 20 mL standard solution of sodium fluoride of different concentrations was added to the centrifugal tube, respectively. The pH of the solution was adjusted to 7.0, with an adsorbent dosage of 1 g/L and the solution was placed in a thermostatic shaking machine to oscillate at 25°C and 150 rpm rotation speed for 24 h. The residual concentration of fluoride in the solution was measured by the fluoride ion-selective electrode. The kinetics studies were carried out under the condition of 25°C and 150 rpm in a constant temperature shaking table for 24 h, with an adsorbent dose of 1 g/L. The 200 mL of fluoride standard solution with the concentration of 10 mg/L was adjusted at pH = 7 and moved into 250 mL of the conical flask. With 0.1 M HCl and NaOH solution to 10 mg/L of sodium fluoride standard solution pH adjustment to a certain gradient range (2.0~11.0) to provide different pH conditions at 25°C and an adsorbent dose of 1 g/L. The experiment of the interference adsorption effect of co-existing ions was carried out. Sodium chloride, sodium nitrate, sodium sulfate, sodium bicarbonate, and sodium phosphate at three kinds of concentrations (0.1, 1.0, and 10 mol/L) were added to the sodium fluoride solution of 10 mg/L at pH = 7, the temperature of 25°C, and an adsorbent dose of 1 g/L. And the defluorination efficiency of co-existing ions of various concentrations was calculated. For evaluating the regeneration of adsorbents, fluoride-adsorbed FAN was soaked into sodium hydroxide solution (3 wt.%) for use again. Six consecutive adsorption–desorption cycles were performed to explore the regeneration of the FAN adsorbent.

3. Results and discussion

3.1. Sample characterization

The crystal structures of the final products were analyzed by powder X-ray diffractometric analysis shown in Fig. 1. It shows that the peaks at the 2θ of 31.79°, 45.53°, and 66.36° can be attributed to (220), (400), and (440) planes of the Al_2NiO_4 (JCPDS card no. 01-073-0239), and the peaks at the 2θ of 56.56° and 75.37° can be indexed to (333) and (444) planes of magnetic Fe_3O_4 (JCPDS card no. 01-086-1352). Obviously, the Fe-Al-Ni composite metal oxide was successfully prepared and the characteristic peak strength was high, indicating that the crystallinity of the crystal in the sample was good.

The morphology of FAN nanoparticles can be obtained by SEM, as shown in Fig. 2. Figs. 2a and b are SEM images of FAN metal complex grown by coprecipitation, and Figs. 2c and d are SEM images of the material after fluoride adsorption. The surface of each adsorbent particle is covered with a tiny volume crystal, which basically presents a block-like structure similar to that of a cube. The growth of the crystal is relatively uniform, which size is about 0.2–0.6 μm. The adsorbent has good dispersibility,
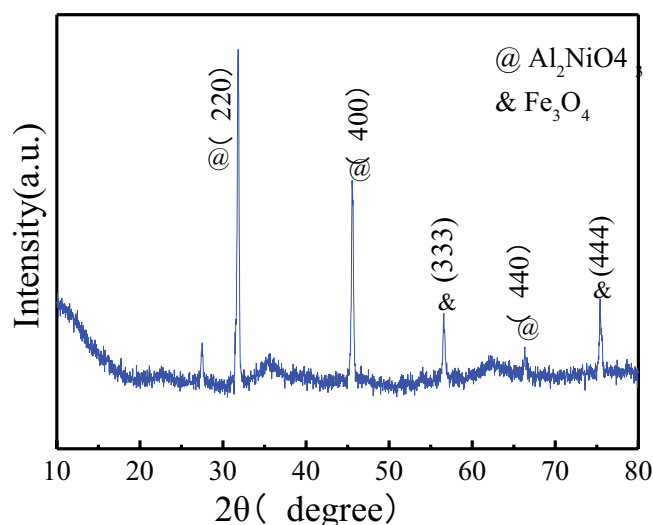

Fig. 1. XRD pattern of FAN composite oxide.

clear particles, and no obvious agglomeration. Small flat crystals on the surface of FAN particles increased the surface area of each particle. After defluorination, the crystal structure on the surface of the particles disappeared, particles showed irregular in size.

As shown in Fig. 3, EDS scanning was conducted to study the elements composition of FAN particles surface after saturated adsorption and whether the material has the ability to absorb F^-. Table 1 shows that the sample $n(Fe):n(Al):n(Ni) \approx 1.6:1.5:1$, which verifies that the molar ratio is close to the previously experimental molar ratio of 1:1:1. After saturated adsorption, the surface contains a large number of fluoride elements, indicating that fluoride elements have been evenly distributed on the adsorbent surface, and can be separated from the solution with the adsorbent.

FT-IR can provide molecular and structural information about organic and inorganic materials [18]. The result of the Fourier transform infrared spectrogram (FT-IR) study of FAN composite oxide before and after fluoride adsorption is shown in Fig. 4. It shows sharp peaks at 620; 707; 1,336; 1,429; 1,558; 1,625; and 2,958 cm^{-1}. After fluoride adsorption, there is a slight shift of peaks at 435; 622; 711; 1,334; 1,425; 1,564; 1,629; and 2,960 cm^{-1}. The peak at 435 cm^{-1} was assigned to hydrous metal oxides [19]. The peak at 622 cm^{-1} is related to the tensile vibration of the Fe–O bond in materials [20], and the peak at 711 cm^{-1} can be attributed to the bending vibration of the Al–O bond. The emerging band at 1,334 cm^{-1} is attributed to the vibration of F^-. A general slight shift of frequency is attributed to F^- ions adsorbed to FAN [21]. The peak at 1,629 cm^{-1} corresponds to O–H bending vibration [22], while the peak at 2,960 cm^{-1} is caused by C–H stretching vibration. The FT–IR study confirmed that the F^- ion has a strong binding ability with the surface of the FAN composite oxide adsorbent.

To study the zero point pH_{pzc} of FAN composite oxide, zeta potentials of adsorbent before and after adsorption of fluorine at different pH were measured. As shown in Fig. 5, pH_{pzc} of FAN composite oxide before adsorption is 8.60. When adsorbing fluorine ions, the adsorbent surface with a
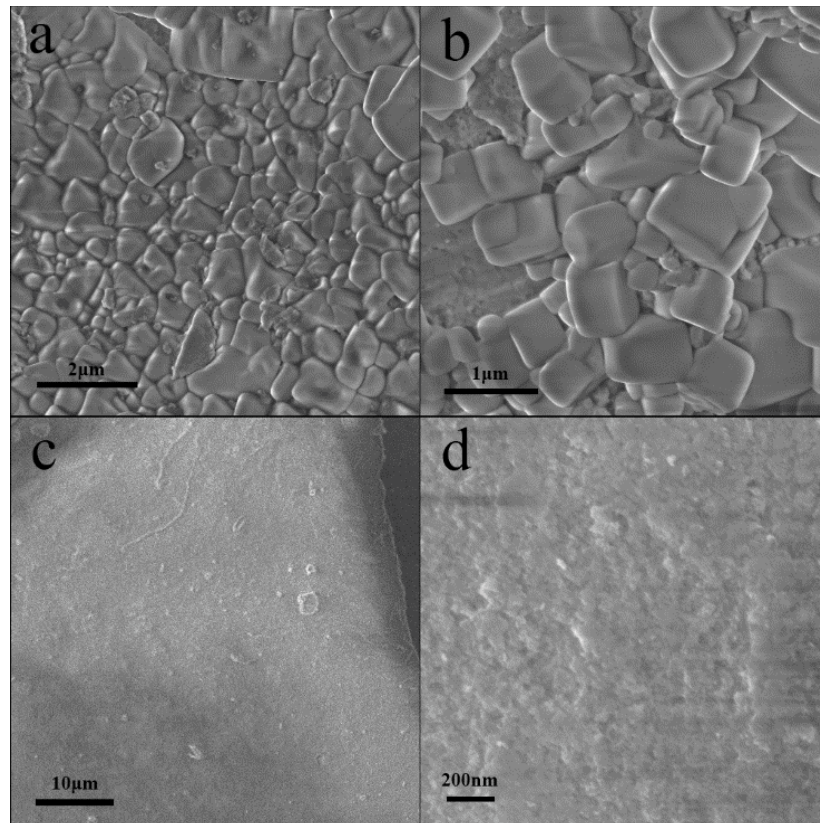
Fig. 2. SEM images of FAN composite oxide: (a and b) before adsorption and (c and d) after adsorption.

Fig. 3. EDS pattern of FAN composite oxide after adsorption.

Table 1
Elemental composition of the synthesized FAN composite oxide after adsorption

Elements	F K	Fe K	Al K	Ni K	Total
Weight%	0.29	0.43	0.22	0.30	2.43
Atomic%	13.7	6.93	7.47	4.63	32.7

positive charge is more favorable for adsorption. When pH is 2~4, the zeta potential value of the adsorbent surface is higher, and the potential value also transits from positive value to negative value during the subsequent change of pH from low to high. Because fluoride ion is negatively charged, the attraction of FAN composite oxide gradually turns to repulsion. This phenomenon also explains the high fluoride removal efficiency of adsorbents in an acidic environment and the significant decrease in fluoride removal efficiency in an alkaline environment in the study of the effect of pH on FAN adsorption. It can be concluded that the adsorption of fluoride ions by FAN is based on a higher zero-point potential, so that it has a strong electrostatic attraction to fluoride ions in the aqueous solution, combined with the hydroxyl exchange effect, to achieve a good fluoride removal effect.
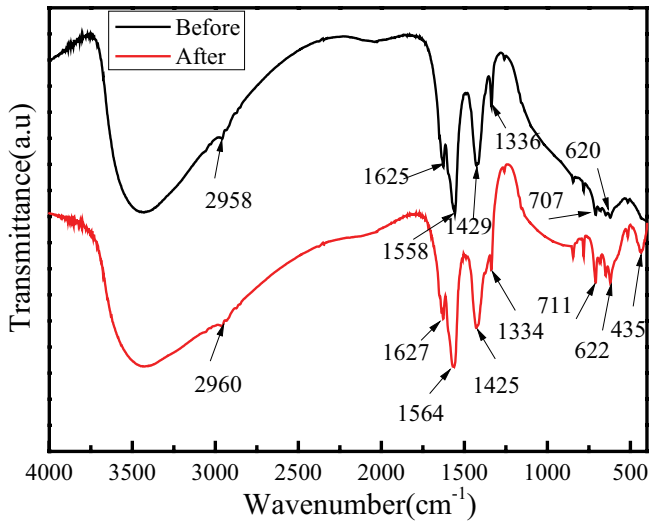
Fig. 4. FT-IR spectra of FAN composite oxide before and after fluoride adsorption.
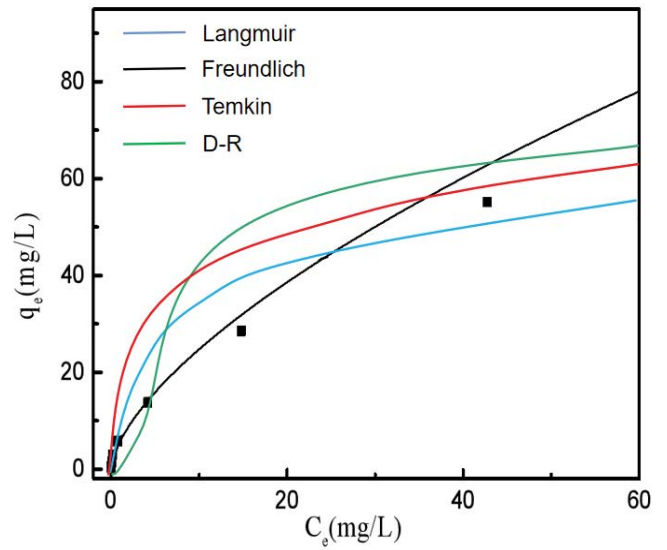

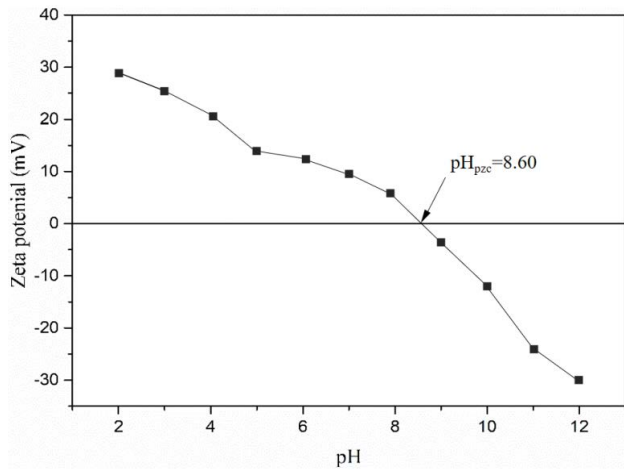Fig. 6. Isotherm of fluoride adsorption by FAN composite oxide.

Fig. 5. Zeta potential of FAN composite oxide before and after defluorination at different pH.

3.2. Adsorption isotherm

To investigate the adsorption performance and the adsorption mechanism, the adsorption isotherms experiments were conducted. There are four commonly used isotherm models namely Langmuir (4), Freundlich (5), Temkin (6), and Dubinin–Radushkevich (7) were used in the presented study.

$$\frac{C_e}{q_e} = \frac{C_e}{q_m} + \frac{1}{K_L q_m} \tag{4}$$

$$\ln q_e = \frac{1}{n}\ln C_e + \ln K_F \tag{5}$$

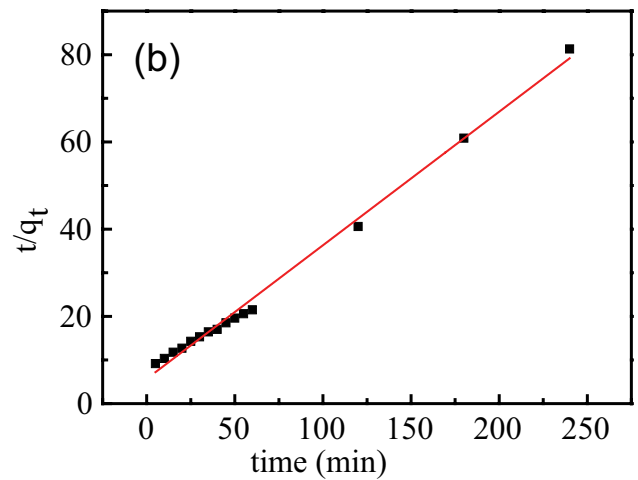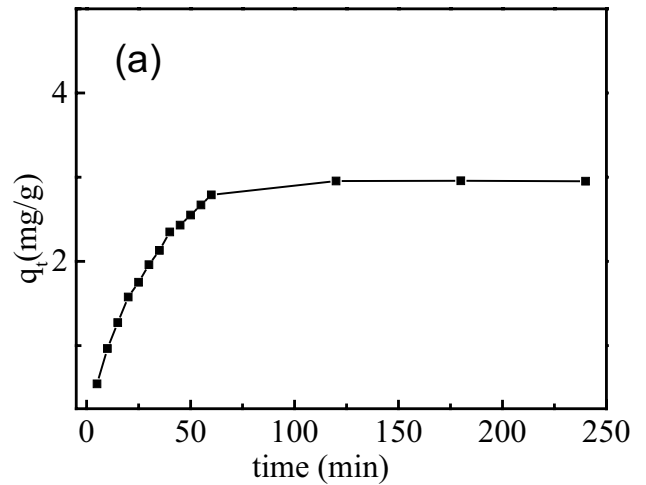$$q_e = \frac{RT}{B_t}\ln K_T C_e \tag{6}$$

Fig. 7. Plot for the (a) experimental data of the kinetics of fluoride removal and (b) pseudo-second-order kinetic fitting of fluoride adsorption.

$$q_e = q_m \exp\left(-K_{DR}\varepsilon^2\right) \tag{7}$$

where C_e (mg/L) is the fluorine concentration after equilibrium adsorption; q_e (mg/g) is the amount of defluoridation on per weight of the adsorbent after equilibrium; q_m (mg/g) is the maximum adsorption capacity calculated according to Langmuir equation; K_L (L/mg) is the Langmuir adsorption constant; K_F (mg/g), and n are Freundlich adsorption constant. The K_T represents the Temkin isotherm constant (L/g) and B_t is binding energy constant (J/mol); T is the temperature, R is the universal gas constant (8.314 J/kmol), K_{DR} is the D–R isotherm constant (mol²/kJ²), ε represents the Polanyi potential ($\varepsilon = RT\ln[1 + 1/C_e]$), and E is the so-called characteristic energy of adsorption ($E = \dfrac{1}{\sqrt{2K_{DR}}}$) [23,24].

The experimental adsorption results fitted by Langmuir, Freundlich, Temkin and D-R models are shown in Fig. 6. The corresponding parameters of the four models are summarized in Table 2. It suggested that the adsorption of fluoride on FAN was fitted well with the Freundlich model based on the values of correlation coefficient (R^2). When the initial fluoride concentration was 200 mg/L, the maximum adsorption capacity was 55.2 mg/g and the q_{max} value was calculated as 59.5 mg/g from the Langmuir model. The fitting results were consistent with the Freundlich model, indicating that

Table 2
Parameters of Langmuir, Freundlich, Temkin, and D–R adsorption isotherm model

Isotherm model	Parameters	Value
Langmuir	K_L (L/mg)	0.142
	q_{max} (mg/g)	59.5
	R^2	0.872
Freundlich	n	1.56
	K_F	5.67
	R^2	0.931
Temkin	B_t (J/mol)	14.1
	K_T (L/mg)	9.83
	R^2	0.803
D–R	q_m (mg/g)	48.3
	E (kJ/mol)	10.3
	R^2	0.834

the adsorbent was multilayer adsorption with uneven distribution of adsorption sites. The Langmuir and Freundlich isotherm models can't fully explain the adsorption mechanism, so Temkin and D–R isotherm models were fitted into the experimental data [25–27]. The binding energy found from the Temkin isotherm model indicates the electrostatic attraction between the adsorbent and the adsorbate. In this study, the E-value is 10.3 kJ/mol, and the adsorption process can be considered as chemical adsorption. Finally, there are several comparisons of adsorption capacity with various adsorbents are summarized in Table 3.

3.3. Kinetic study

An adsorption kinetic model, usually applied for estimation of adsorption rate, provides valuable insights into the mechanism of adsorption reaction. The experimental data of adsorption kinetics are usually simulated by pseudo-first-order kinetics (8) and pseudo-second-order kinetics (9) models, respectively.

$$\ln\left(q_e - q_t\right) = \ln q_e - k_1 t \tag{8}$$

$$\frac{t}{q_e} = \frac{1}{k_2 q_e^2} + \frac{t}{q_e} \tag{9}$$

where q_e and q_t are the amount of fluoride adsorbed (mg/g) at equilibrium and at any time, respectively; t (min) is the adsorbed time. The k_1 (1/min) is the rate constant for a pseudo-first-order reaction. The k_2 (g/(mg min)) is the rate constant for pseudo-second-order reaction.

The corresponding parameters of the two models are calculated from the plot of $\ln(q_e - q_t)$ vs. t and (t/q_t) vs. t, respectively. Table 4 shows a higher value of correlation coefficients for the pseudo-second-order compared to the first-order-kinetic, which gives a better fit to the experimental data for F⁻ adsorption onto the FAN. According to the pseudo-second-order model shown in Fig. 7, the equilibrium adsorption capacity ($q_{e,cal}$) was calculated as 3.27 mg/g when the initial fluoride concentrations were 10 mg/L, with an adsorbent dose of 1 g/L, pH = 7, the temperature of 25°C, which is closer to the corresponding experimental values ($q_{e,exp}$) of 2.95 mg/g than the pseudo-first-order. It shows that the pseudo-second-order kinetics is able to demonstrate the adsorption kinetic behavior, indicating that there is a strong electrostatic interaction between the adsorbent and fluoride.

Table 3
Comparison on adsorption capacity of different adsorbents

Adsorbents	pH	Temperature (°C)	Adsorption capacity (mg/g)	Ref.
Fe-Ti oxide	7	25	31.2	[28]
Mg-Al bimetallic oxides	6	25	89.3	[29]
CeO₂-ZrO₂ nanocages	4	25	175	[30]
CTAB assisted mixed iron oxide	5	25	40.4	[31]
Zirconium-modified-Na-attapulgite	4.13	50	24.6	[32]
Trititanate nanotubes (TNT)	2	80	58	[33]
FAN	7	25	59.5	Present work

Table 4
Parameters of pseudo-first and second-order kinetics model

Kinetics model Pseudo-first-order			Pseudo-second-order		
k_1 (1/min)	q_e (mg/g)	R^2	k_2 (g/(mg min))	q_e (mg/g)	R^2
0.04	3.42	0.966	0.016	3.27	0.994

Fig. 8. Effect of pH on fluoride adsorption.

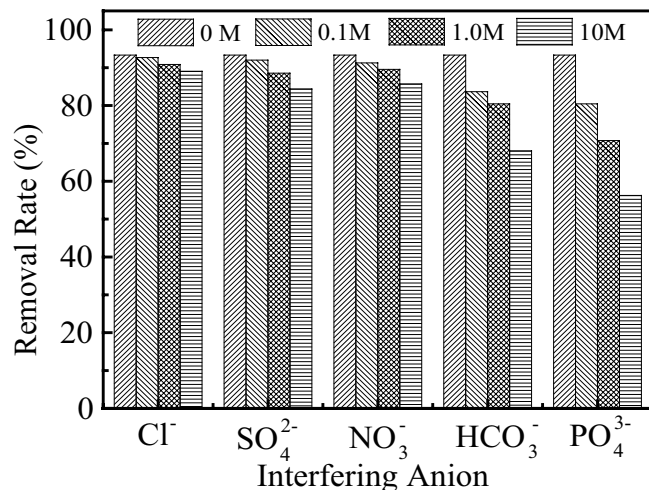Fig. 10. Regeneration test of adsorbent.
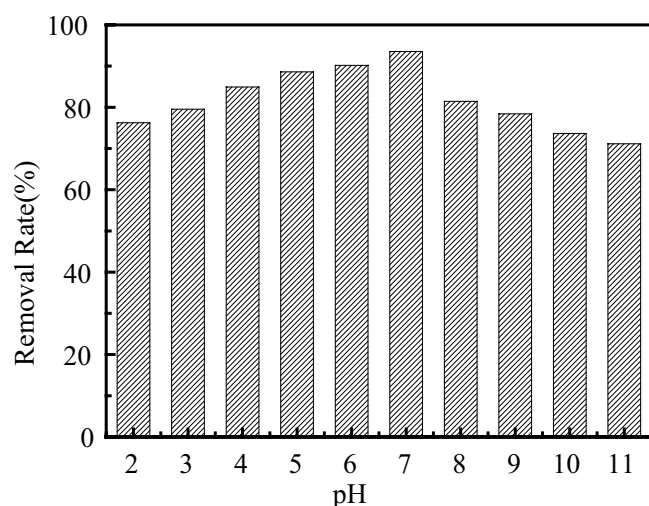
Fig. 9. Effect of co-existing anions on fluoride adsorption.

3.4. Effect of pH on fluoride adsorption

To investigate the defluorination properties of FAN adsorbent by pH. The variation of pH on fluoride adsorption were studied by using 10 different samples having a pH range of 2–11. As shown in Fig. 8, it was found that the maximum removal rate was 93.6% at pH = 7, with an initial fluoride concentration of 10 mg/L. In the acidic pH range, weak hydrofluoric acid (HF) is present in the experiments that may affect defluoridation [34]. However, in the strongly alkaline range, there is a sharp drop in adsorption,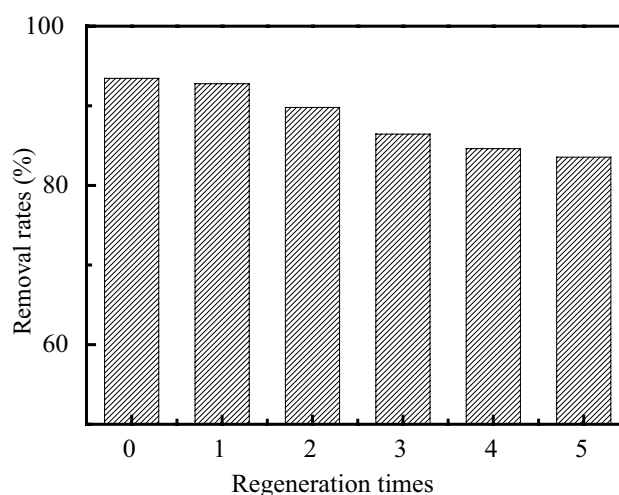 which may be due to the competition of more hydroxyl ions with the fluoride and the electrostatic repulsion from the surface of the adsorbent [35].

3.5. Effect of co-existing anions

To explore the relationship between the fluoride removal efficiency of FAN adsorbent and the types and concentrations of co-existing ions in water, the co-existing ions of chloride, sulfate, nitrate, phosphate, and bicarbonate were studied by the batch method. As shown in Fig. 9, chloride, sulfate, and nitrate don't have much effect on F$^-$ adsorption, but phosphate and carbonate show a significant effect on F$^-$ removal. Both phosphate and carbonate show a significantly higher reduction in F$^-$ adsorption efficiency due to change in pH, as well as the competing effect of this co-ion for the active site of the adsorbent [22,36,37]. The affinity sequence for the anion adsorption on this adsorbent is phosphate > bicarbonate > nitrate > sulfate > chloride. Calculating the distribution coefficient according to Eq. (3), which is beneficial for understanding the affinity of adsorbents to adsorbate molecules [38]. The K_d values for the fluoride-loaded FAN composite oxide are in the range of $(0.8–3.5) \times 10^4$ mL/g. The higher K_d value of the FAN composite indicates that the material has a strong affinity for fluoride.

3.6. Regeneration and reuse of the adsorbent

As shown in Fig. 10, the desorption and regeneration of FAN adsorbent were investigated for six times adsorption–desorption cycles with the initial fluoride concentration of 10 mg/L, pH = 7, the temperature of 25°C, and adsorbent dose of 1 g/L. The removal rates of adsorbents are 93.5%, 92.8%,

89.8%, 86.5%, 84.6%, and 83.6%, respectively. It shows that the efficacy of the adsorbents still maintains high as being reused repeatedly, indicating that the spent adsorbent is suitable for regeneration.

4. Conclusion

The FAN composite oxide was synthesized by the coprecipitation method with a simple preparation process. The adsorbent was characterized by using SEM, XRD, FT-IR, zeta potential, and EDS, and its defluoridation properties were investigated. Adsorption kinetics fitted well the pseudo-second-order model. The fluoride adsorption isotherm was well-demonstrated by the Freundlich model. Moreover, when the initial fluoride concentration was 200 mg/L, the maximum adsorption capacity was calculated as 59.5 mg/g from the Langmuir model. It found that the maximum removal rate was 93.6% at pH = 7, with an initial fluoride concentration of 10 mg/L. The co-existing anions indicate that chloride, sulfate, and nitrate don't have much effect on F^- adsorption, but phosphate and carbonate show a significant effect on F^- removal. It shows that the efficacy of the adsorbents still maintains high as being reused, indicating that the spent adsorbent is suitable for regeneration. These research results indicate that the adsorbent of FAN composite oxide can be potentially suitable materials used in fluoride removal.

References

[1] G. Biswas, M. Kumari, K. Adhikari, S. Dutta, A critical review on occurrence of fluoride and its removal through adsorption with an emphasis on natural minerals, Water Pollut., 3 (2017) 104–119.

[2] B.F. Alien, A.L. Nubia, P.G. Víctor, M.G. José, O.E. María, R.T. Israel, Efficient fluoride removal using Al–Cu oxide nanoparticles supported on steel slag industrial waste solid, Environ. Sci. Pollut. Res., 25 (2017) 1–15.

[3] G.V. Patankar, A.S. Tambe, B.D. Kulkarni, A. Malyshew, S.P. Kamble, Defluoridation of drinking water using pural®MG-20 mixed hydroxide adsorbent, Water Air Soil Pollut., 224 (2013) 545–557.

[4] L.D. Kong, J.X. He, A.Y. Wang, H. Li, The progress of the research on the treatment of the fluorine-containing sewage, Sci. Technol. Inf. Dev. Econ., 16 (2006) 46–48.

[5] S.V. Jadhav, K.V. Marathe, V.K. Rathod, A pilot scale concurrent removal of fluoride, arsenic, sulfate and nitrate by using nanofiltration: competing ion interaction and modelling approach, J. Water Process Eng., 13 (2016) 153–167.

[6] H.B. Cong, F. Sun, W.J. Chen, Y.J. Xu, W. Wei, Study on the method and mechanism of pre-pressure coagulation and sedimentation for microcystis removal from drinking-water sources, Environ. Technol., 39 (2018) 433–449.

[7] A.R. Donovan, C.D. Adams, Y.F. Ma, C. Stephan, T. Eichholz, H.L. Shi, Fate of nanoparticles during alum and ferric coagulation monitored using single particle ICP-MS, Chemosphere, 195 (2017) 531–541.

[8] E. Bazrafshan, K.A. Ownagh, A.H. Mahvi, Application of electrocoagulation process using iron and aluminum electrodes for fluoride removal from aqueous environment, J. Chem., 9 (2012) 2297–2308.

[9] F.D. Belkada, O. Kitous, N. Drouiche, S. Aoudj, O. Bouchelaghem, N. Abdi, H. Grib, N. Mameri, Electrodialysis for fluoride and nitrate removal from synthesized photovoltaic industry wastewater, Sep. Purif. Technol., 204 (2018) 108–115.

[10] I. Parlar, M. Hacıfazlıoğlu, N. Kabay, T.Ö. Pek, M. Yüksel, Performance comparison of reverse osmosis (RO) with integrated nanofiltration (NF) and reverse osmosis process for desalination of MBR effluent, J. Water Process Eng., 29 (2019) 100640, doi: 10.1016/j.jwpe.2018.06.002.

[11] D.J. Kang, X.L. Yu, M.F. Ge, Morphology-dependent properties and adsorption performance of CeO_2 for fluoride removal, Chem. Eng. J., 330 (2017) 36–43.

[12] Y.X. Zhang, Y. Jia, Fluoride adsorption on manganese carbonate: ion-exchange based on the surface carbonate-like groups and hydroxyl groups, J. Colloid Interface Sci., 510 (2017) 407–417.

[13] A.A. Markeb, A. Alonso, A. Sánchez, X. Font, Adsorption process of fluoride from drinking water with magnetic core-shell Ce-Ti@Fe_3O_4 and Ce-Ti oxide nanoparticles, Sci. Total Environ., 598 (2017) 949–958.

[14] S. George, P. Pandit, A.B. Gupta, Residual aluminium in water defluoridated using activated alumina adsorption-modeling and simulation studies, Water Res., 44 (2010) 3055–3064.

[15] X.L. Zhao, J.M. Wang, F.C. Wu, T. Wang, Y.L. Cai, Y.L. Shi, G.B. Jiang, Removal of fluoride from aqueous media by Fe_3O_4@$Al(OH)_3$ magnetic nanoparticles, J. Hazard. Mater., 173 (2010) 102–109.

[16] L.Y. Chai, Y.Y. Wang, N. Zhao, W.C. Yang, X.Y. You, Sulfate-doped Fe_3O_4/Al_2O_3 nanoparticles as a novel adsorbent for fluoride removal from drinking water, Water Res., 47 (2013) 4040–4049.

[17] K. Mukhopadhyay, A. Ghosh, S.K. Das, Synthesis and characterisation of cerium(IV)-incorporated hydrous iron(III) oxide as an adsorbent for fluoride removal from water, RSC Adv., 7 (2017) 26037–26051.

[18] M. Kamranifar, A. Naghizadeh, Montmorillonite nanoparticles in removal of textile dyes from aqueous solutions: study of kinetics and thermodynamics, Iran. J. Chem. Chem. Eng., 36 (2017) 127–137.

[19] K. Biswas, S.K. Saha, U.C. Ghosh, Adsorption of fluoride from aqueous solution by a synthetic iron(III)-aluminum(III) mixed oxide, Ind. Eng. Chem. Res., 46 (2007) 5346–5356.

[20] M. Kumar, G. Vijayakumar, R. Tamilarasan, Synthesis, characterization and experimental studies of nano Zn-Al-Fe_3O_4 blended alginate/Ca beads for the adsorption of Rhodamin B, J. Polym. Environ., 27 (2018) 106–117.

[21] S. Raghav, D. Kumar, Adsorption equilibrium, kinetics, and thermodynamic studies of fluoride adsorbed by tetrametallic oxide adsorbent, J. Chem. Eng. Data, 63 (2018) 1682–1697.

[22] W. Xiang, G.K. Zhang, Y.L. Zhang, D.D. Tang, J.T. Wang, Synthesis and characterization of cotton-like Ca-Al-La composite as an adsorbent for fluoride removal, Chem. Eng. J., 250 (2014) 423–430.

[23] U.K. Sahu, S. Sahu, S.S. Mahapatra, R.K. Patel, Synthesis and characterization of magnetic bio-adsorbent developed from *Aegle marmelos* leaves for removal of As(V) from aqueous solutions, Environ. Sci. Pollut. Res., 26 (2019) 946–958.

[24] S. Sahu, U.K. Sahu, R.K. Patel, Modified thorium oxide polyaniline core-shell nanocomposite and its application for the efficient removal of Cr(VI), J. Chem. Eng. Data, 64 (2019) 1294–1304.

[25] S. Sahu, S. Pahi, S. Tripathy, S.K. Singh, A. Behera, U.K. Sahu, R.K. Patel, Adsorption of methylene blue on chemically modified lychee seed biochar: dynamic, equilibrium, and thermodynamic study, J. Mol. Liq., 315 (2020) 1–41, doi: 10.1016/j.molliq.2020.113743.

[26] S. Sahu, S. Pahi, J.K. Sahu, U.K. Sahu, R.K. Patel, Kendu (Diospyros melanoxylon Roxb) fruit peel activated carbon—an efficient bioadsorbent for methylene blue dye: equilibrium, kinetic, and thermodynamic study, Environ. Sci. Pollut. Res., 27 (2020) 22579–22592.

[27] S. Sahu, P. Kar, N. Bishoyi, L. Mallik, R.K. Patel, Synthesis of polypyrrole-modified layered double hydroxides for efficient removal of Cr(VI), J. Chem. Eng. Data, 64 (2019) 4357–4368.

[28] L. Chen, B.Y. He, S. He, T.J. Wang, C.L. Su, Y. Jin, Fe–Ti oxide nano-adsorbent synthesized by co-precipitation for fluoride removal from drinking water and its adsorption mechanism, Powder Technol., 227 (2012) 3–8.

[29] S. Moriyama, Mg–Al bimetallic oxides as sorbents for the removal of F^- in aqueous solutions, Chemosphere, 95 (2014) 597–603.

[30] J. Wang, W.H. Xu, L. Chen, Y. Jia, L. Wang, X.J. Huang, J.H. Liu, Excellent fluoride removal performance by CeO_2-ZrO_2 nanocages in water environment, Chem. Eng. J., 231 (2013) 198–205.

[31] M. Mohapatra, K. Rout, P. Singh, S. Anand, S. Layek, H.C. Verma, B.K. Mishra, Fluoride adsorption studies on mixed-phase nano iron oxides prepared by surfactant mediation-precipitation technique, J. Hazard. Mater., 186 (2011) 1751–1757.

[32] G.K. Zhang, Z.L. He, W. Xu, A low-cost and high efficient zirconium modified Na attapulgite adsorbent for fluoride removal from aqueous solutions, Chem. Eng. J., 183 (2012) 315–324.

[33] P. Chinnakoti, R.K. Vankayala, A.L.A. Chunduri, L.R. Nagappagari, S.V. Muthukonda, V. Kamisetti, Trititanate nanotubes as highly efficient adsorbent for fluoride removal from water: adsorption performance and uptake mechanism, J. Environ. Chem. Eng., 4 (2016) 4754–4768.

[34] A.M. Raichur, M.J. Basu, Adsorption of fluoride onto mixed rare earth oxides, Sep. Purif. Technol., 24 (2001) 121–127.

[35] K.S. Zhang, S.B. Wu, X.L. Wang, J.Y. He, L.T. Kong, J.H. Liu, Wide pH range for fluoride removal from water by MHS-MgO/$MgCO_3$ adsorbent: kinetic, thermodynamic and mechanism studies, J. Colloid Interface Sci., 446 (2015) 194–202.

[36] S. Sahu, U.K. Sahu, R.K. Patel, Synthesis of thorium-ethanolamine nanocomposite by co-precipitation method and its application for Cr(VI) removal, New J. Chem., 42 (2018) 5556–5569.

[37] U.K. Sahu, S. Sahu, S.S. Mahapatra; R.K. Patel, Cigarette soot activated carbon modified with Fe_3O_4 nanoparticles as an effective adsorbent for As(III) and As(V): material preparation, characterization and adsorption mechanism study, J. Mol. Liq., 243 (2017) 395–405.

[38] S. Sahu, L. Mallik, S. Pahi, B. Barik, U.K. Sahu, M. Sillanpää, R.K. Patel, Facile synthesis of poly o-toluidine modified lanthanum phosphate nanocomposite as a superior adsorbent for selective fluoride removal: a mechanistic and kinetic study, Chemosphere, 252 (2020) 1–13, doi: 10.1016/j.chemosphere.2020.126551.